ChemComm

Mapping the supramolecular assembly space of poly(sarcosine)-b-poly(propylene sulfide) using a combinatorial copolymer library

Journal:	*ChemComm*
Manuscript ID	CC-COM-02-2020-000925.R1
Article Type:	Communication

COMMUNICATION

Mapping the supramolecular assembly space of poly(sarcosine)-*b*-poly(propylene sulfide) using a combinatorial copolymer library

Received 00th January 20xx,
Accepted 00th January 20xx

DOI: 10.1039/x0xx00000x

Molly Frey,[a] Mike Vincent,[b] Sharan Bobbala,[b] Rajan Burt,[b] and Evan Scott[a,b]

A combinatorial copolymer library was created to rapidly screen the landscape of self-assembed nanostructure morphologies formed by block copolymers composed of hydrophilic peptoid polysarcosine (PSarc) and hydrophobic poly(propylene sulfide) (PPS) blocks. By probing rationally selected hydrophilic/ hydrophobic copolymer weight fractions, the rapid and reproducible fabrication of micellar and vesicular nanostructures was optimized.

One major challenge in the development of novel self-assembled bionanomaterials is evaluating whether block copolymer constructs are capable of stably forming a useful nanocarrier morphology in aqueous environments. The assembled morphology is highly dependent on the ratio of hydrophilic to hydrophobic blocks, as well as the specific chemistry and functionalization.[1] The impact of these variables on the self-assembly process can be estimated through thermodynamic modeling and molecular dynamics simulations. However, these computational approaches are rarely capable of predicting the true final assembled aggregate morphology and its associated supramolecular properties.[2,3] Alternatively, an experimental screening pipeline could facilitate the development and testing of novel polymer prototypes for minimal time, cost, and quantity. This evaluation process must be (1) comprehensive to minimize false negatives, and (2) rapid to quickly halt further development of dysfunctional prototypes that fail to meet the defined self-assembly criteria. Importantly, this pipeline must achieve these development goals without sacrificing the rigorous characterization of the material properties being screened. It is with this motivation that we sought to create a robust pipeline that utilizes a combinatorial approach to rapidly and efficiently probe nanoparticle characteristics across an otherwise extensive range of copolymer prototypes that varied in their hydrophilic block weight fractions. Furthermore, this approach allows for the customization of polymer chemistry to overcome downstream difficulties that often arise at the blood-polymer interface, principally protein adsorption and rapid clearance by the immune system.[4] Here, we developed and employed such a pipeline to evaluate and optimize the self-assembly of a novel poly(sarcosine)-*b*-poly(propylene sulfide) (PSarc-*b*-PPS) diblock copolymer as a new class of NCA-*b*-PPS polymer for nanostructures desirable for applications in controlled drug delivery.

Poly(propylene sulfide) (PPS) is a non-toxic and highly versatile hydrophobic polymer that forms stable lyotropic mesophases in aqueous solution.[5] It is often selected as the hydrophobic block for self-assembled nanocarriers due to the sensitivity of its repeated sulfide units to oxidation that generates hydrophilic sulfoxide and sulfone moieties.[6] These hydrophilic derivatives result in rapid disassembly of the aggregate structure for both on-demand drug delivery as well as clearance of the material through the kidneys, which is an advantage over alternative hydrophobic blocks like polystyrene that can instead remaining present within the circulation or tissues.[5,7] Nanostructures assembled from copolymers containing PPS hydrophobic blocks are able to trigger intracellular release after cellular uptake into oxidizing endo-lysosomes.[8] Additional evidence suggests that the PPS block can also temporarily permeabilize the lysosomal membrane and allow for cytosolic release of therapeutic cargo.[8] Furthermore, the low glass transition temperature of PPS permits rapid reorganization of hydrophobic domains during self-assembly, enabling the stable formation of diverse nanostructures using scalable self-assembly techniques like flash nanoprecipitation (FNP).[9,10] PPS can be quickly and inexpensively synthesized through the initiation of commercially available propylene sulfide by a small-molecule thiolate ion. Materials incorporating PPS polymer have been utilized successfully in drug delivery systems and are non-toxic in nonhuman primates, making this hydrophobic block a promising option for a novel self-assembling PSarc-based material.[11]

N-carboxyanhydride (NCA) polymers are especially attractive options for the development of biomimetic materials, since the resulting peptide backbone formed between amino acid monomer units closely resembles endogenous peptides in a similar capacity to solid phase peptide synthesis. Additionally, the ring-opening polymerization (ROP) of NCA monomers with a primary amine is conducted under mild, easily controlled conditions to yield polymer populations of reliable dispersity.[12] The monomers themselves offer

[a] *Interdisciplinary Biological Sciences, Northwestern University, Evanston, IL*
[b] *Department of Biomedical Engineering, Northwestern University, Evanston, IL*
† *Corresponding Author: Evan Scott, PhD, Assistant Professor of Biomedical Engineering, Northwestern University, 2145 Sheridan Road, Evanston, IL 60208, evan.scott@northwestern.edu*
Electronic Supplementary Information (ESI) available: [details of any supplementary information available should be included here]. See DOI: 10.1039/x0xx00000x

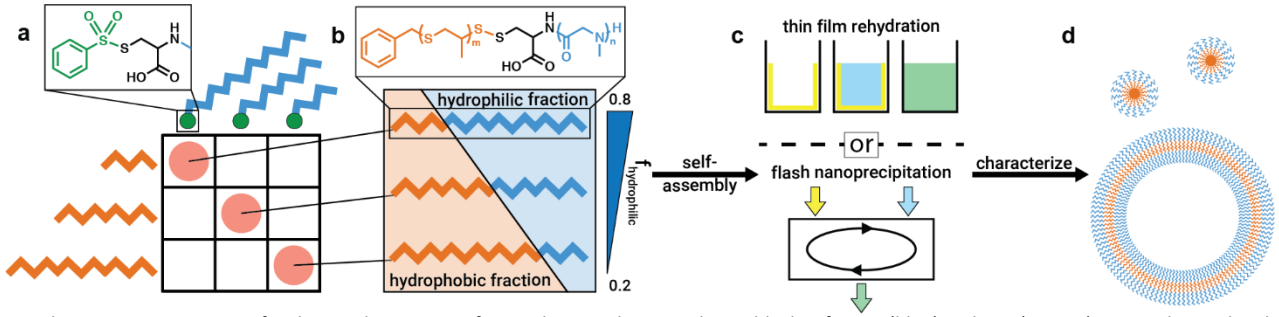

Fig. 1 Schematic representation for the rapid screening of PSarc-*b*-PPS polymer. Polymer blocks of PSarc (blue) and PPS (orange) are synthesized with an phenylthiosulfate-cysteine linker (green) and paired across a combinatorial library (a) to cover the full range of relevant f_{PSarc} (b). The diblock copolymers are subjected to self-assembly thin film rehydration or flash nanoprecipitation (c). The stabilized nanostructures are characterized to determine the morphological properties of each population (d).

a vast range of modular functionalization as each heterocyclic ring can accommodate a unique side chain without significantly altering the polymerization chemistry. This allows for the incorporation of functional groups found in the 20 natural amino acids as well as a virtually unlimited number of non-canonical derivatives.[13] Finally, polymers formed from NCA monomers maintains a primary amine terminal end, which can be utilized for any of the existing conjugation strategies to biological substrates or further chemical modifications.

Sarcosine, i.e. N-methyl glycine, is the simplest NCA-derived monomer and conserves the broad chemical properties of peptide backbones while minimizing side chain complexities. Polymerization of poly(sarcosine) (PSarc) has previously been shown to resist protein adsorption similarly to poly(ethylene glycol) (PEG)[14] and effectively shield charges on nanocarriers like liposomes.[15] To the best of our knowledge, diblock copolymers formed from PSarc and PPS have not been previously synthesized or employed for nanomaterial fabrication. Thus the optimal hydrophilic/hydrophobic weight fractions required to reproducibly assemble useful nanostructure morphologies from such a copolymer are unknown. Furthermore, previous work with self-assembling PSarc copolymers demonstrated vesicle formation at hydrophilic weight fractions (f_{PSarc}) of 0.18 [P(TPE-NAG)$_{25}$-*b*-PSar$_{46}$],[16] 0.54 (GA-PSar$_{43}$-PMLG$_{18}$),[17] and 0.86 (PLLA$_{25}$-PSarc$_{150}$).[18] This formation of a single morphology from such a wide range of f_{PSarc} shows that distinct PSarc copolymers can have drastically different tendencies for nanostructure self-assembly. Using PSarc as a minimal NCA placeholder, we therefore employed a pipeline to systematically establish baseline f_{PSarc} ranges for self-assembly of distinct nanostructures from NCA-*b*-PPS copolymers.

Different lengths of PSarc and PPS blocks were combinatorially paired (Fig. 1a) to produce five copolymers spanning a range of f_{PSarc} using minimal material (Fig. 1b). The copolymers were subjected to thin film rehydration (TF) or FNP for self-assembly (Fig. 1c). The resulting formulations were then characterized by dynamic light scattering (DLS) to measure nanostructure diameter and polydispersity, electrophoretic light scattering (ELS) to measure zeta potential, transmission electron microscopy (TEM) for structural visualization, and small-angle x-ray scattering (SAXS) for an extensive investigation of morphological characteristics (Fig. 1d). Finally, we examined cytotoxicity of the formed nanostructures to ensure that the baseline chemical character of PSarc-*b*-PPS nanomaterials do not induce unintended cell death.

A critical component of this strategy is the selection of a protected linker between the blocks that enables unrestricted pairing of distinct chain lengths of PSarc and PPS. This will maximize the utility of each synthesized polymer and minimize the mass of material needed to conduct the screen. We began exploring potential heterobifunctional linkers beginning with small molecules that could potentially initiate one or both of these chains. Unfortunately, a large number of these candidates failed to adequately isolate the nucleophilic requirements of amines and thiolates and limit ROP to only one end of the polymer at a time (Table S1). As a result, the majority of our initial trials yielded homopolymers extending off both sides of the heterobifunctional initiator. The inability to avoid this cross-reactivity resulted in polymers that did not maintain initiation capability on the opposite end, eliminating any possible use as a linker for future steps.

We therefore selected a cysteine initiator with side chain protection from the phenylthiosulfate moiety, previously shown to be selectively susceptible to thiolate ions over amines.[19] Collectively, this initiator offers both a primary amine on the amino end of the cysteine for NCA initiation as well as a disulfide bond to end cap the thiolate of PPS chains. These three components were incorporated as shown in Scheme S1. The selected blocks suit a maximally efficient approach given the undesirable use of phosgene to synthesize the monomers and the added complexities of N-methylation on a ROP mechanism with a secondary instead of a primary amine.[20]. Hydrophilic PSarc chains of lengths 22 and 29 were synthesized for this library and validated using NMR. These PSarc lengths were matched with hydrophobic PPS unit lengths of 25, 35, and 62 to achieve a copolymer library with an fPSarc ranging from 0.25 to 0.52.

Rational selection of these weight fractions was based on our prior work with the self-assembly of PEG-*b*-PPS copolymers.[7,11] These specific ranges have known morphological significance when subjected to self-assembly in aqueous conditions via TF or FNP. For example, PEG-*b*-PPS vesicular morphologies reliably formed via FNP around the f_{PEG} 0.21 to 0.31 range while filamentous and spherical micellar morphologies formed at 0.38 and higher.[10] This is also consistent with previous studies showing triblock combinations of PEG-*b*-PPS polymer to form vesicles via TF at f_{PEG} 0.20 to 0.30, cylindrical morphologies from f_{PEG} 0.30 to 0.42, and micelles at f_{PEG} 0.43 and above.[21] In this work, we synthesized PSarc-*b*-PPS polymers with a f_{PSarc} between 0.25 and 0.52 for distinguishing between

micellar, vesicular, and potentially worm-like nanostructures (Table 1, Tables S2-S6). PPS lengths were maintained between 20-75 units to ensure retention of oxidation-responsive characteristics that we have validated in our prior work for controlled delivery applications.[22-25]2

Nanocarrier morphology is highly dependent on the method of assembly, as the local interactions between material components and external conditions dictate supramolecular organization. For example, delicate filomicelle assemblies are more amenable to gentle TF strategies while the cubic internal architecture of bicontinuous nanospheres have been observed following high energy regimes including FNP and sonication.[21,24,26] Utilizing multiple assembly methods allowed us to better evaluate which nanostructure morphologies are attainable with the specified polymer under a broa d set of formation conditions. In this way, the pipeline provides a more complete understanding of polymer self-assembly capability, preventing early termination of copolymer prototypes that fail to form nanostructures under one condition but not another. Here, all five copolymer preparations aggregated following TF, but formed stable suspensions after FNP using the same THF:Milli-Q water solvent system (Fig. S5 & S6, Table S6 & S7).

The FNP formulations were characterized by DLS and zeta potential, showing a distinct trend in the development of a second independent population as the f_{PSarc} decreases (Fig. 2). The formations of higher f_{PSarc} copolymers (0.52 and 0.44) have a single, monodisperse population from 32 to 43 nm, a range consistent with a micellar morphology. As the hydrophilic weight fraction decreases and the packing of polymer chains shifts, a second population around 91 to 105 nm begins to appear, indicating a second independent morphology from the smaller peak. For all five polymer samples, the slightly negative zeta potential of -3.82 to -8.37 mV is expected of the PSarc-*b*-PPS chemistry and indicates overall structural stability.

TEM of the negatively stained soft structures shows the existence of populations consistent with the hydrodynamic diameters indicated by DLS (Fig. 2b-f). The micrographs further support unique morphological characteristics between the larger and smaller populations based on the appearance of spherical structures with aqueous lumens, where collapse is often readily visible. In the larger f_{PSarc} of 0.52 and 0.44, the monodisperse smaller diameter structures show spherical centers absent of stain, suggestive of micelles. In the smaller f_{PSarc} of 0.38 to 0.25, the additional larger diameter structures among the micelles have dark spherical centers consistent with a vesicular morphology (polymersomes) having an aqueous lumen capable of collapsing and pooling the dark uranyl formate stain during sample preparation.

Table 1 Parameters and characterization of PSarc-*b*-PPS polymers.

			DLS/ELS				TEM	SAXS[d]		
	f	M_n[a]	*d*	*PDI*	*ZP*	d_{peak}[b]	*ID*[c]	r_{core}	r_{shell}	χ^2
$PSarc_{29}$-*b*-PPS_{25}	0.52	3909	33.5	0.087	-8.37	32	MC	14.9	5.1	cs
$PSarc_{29}$-*b*-PPS_{35}	0.44	4649	44.7	0.196	-8.34	43	MC	19.4	4.5	cs
$PSarc_{22}$-*b*-PPS_{35}	0.38	4125	60.8	0.432	-6.90	37 91	MC PS	17.9 ---	6.8 ---	cs ---
$PSarc_{29}$-*b*-PPS_{62}	0.31	6647	80.9	0.767	-3.82	37 105	MC PS	--- 54.9	--- 7.5	--- v
$PSarc_{22}$-*b*-PPS_{62}	0.25	6150	85.9	0.492	-7.48	32 105	MC PS	--- 55.1	--- 8.2	--- v

[a]M_n was calculated from ^{1}H-NMR. [b]D_{peak} is to describe more clearly the DLS samples with multiple populations and high PDI. [c]TEM visual identification as micelle (MC) or polymersome (PS). [d]SAXS scattering for majority population; χ2 refers to best fitting model as core-shell (cs) or vesicle (v). Labels: d = diameter (nm); PDI = polydispersity index; ZP = zeta potential (mV); d_{peak} = diameter of population peaks (nm); r_{core} = core radius (nm); r_{shell} = shell radius (nm).

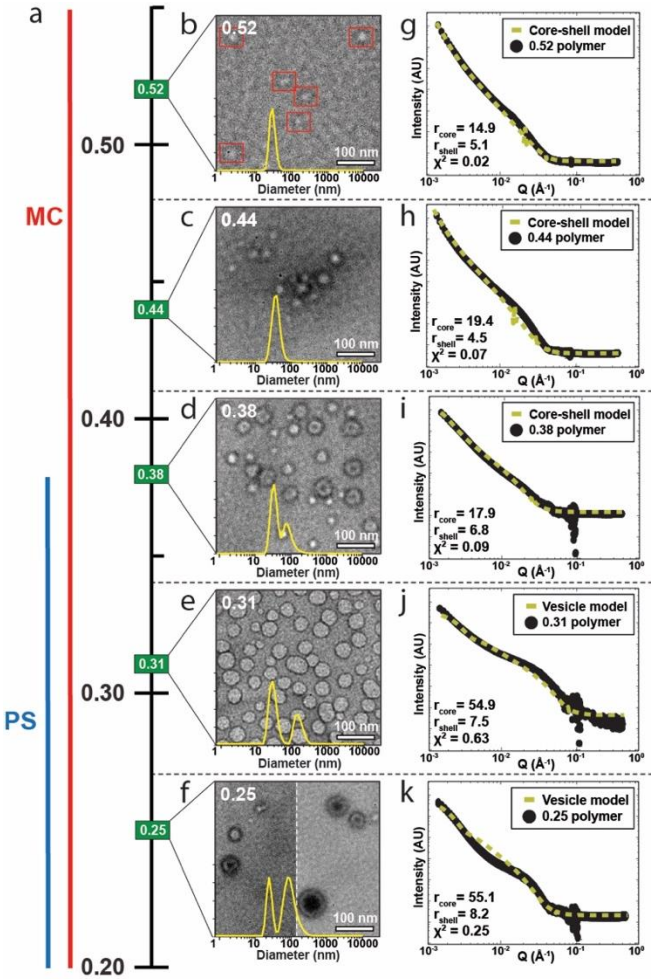

Fig 2 Graphical correlation between the hydrophilic weight fraction and the resulting micelle (MC, red line) or polymersome (PS, blue line) morphology (a). Representative TEM micrographs are shown for each copolymer sample (b-f) with the corresponding number-weighted DLS trace (inset). SAXS scattering profiles were overlayed with the best fitting scattering model (g-k) along with calculated χ^2 values and radii (inset). These orthogonal techniques were used to analyze polymers $PSarc_{29}$-*b*-PPS_{25} (f_{PSarc} = 0.52; b, g*), $PSarc_{29}$-*b*-PPS_{35} (f_{PSarc} = 0.44; c, h), $PSarc_{22}$-*b*-PPS_{35} (f_{PSarc} = 0.38; d, i), $PSarc_{29}$-*b*-PPS_{62} (f_{PSarc} = 0.31; e, j), and $PSarc_{22}$-*b*-PPS_{62} (f_{PSarc} = 0.25; f, k). Due to difficulty in staining of f_{PSarc} 0.52, MC are identified with red squares for improved visualization.

SAXS with synchrotron radiation was performed on these samples to definitively elucidate their morphological characteristics. The calculated radii for each of the five polymer samples were again consistent with the values found through DLS and TEM (Table 1). The scattering profiles of samples with f_{PSarc} of 0.52, 0.44, and 0.38 fit the core-shell sphere model (Fig. 2g-i), presenting strong correlating evidence for a micelle-type structure of these particles. Additionally, the scattering profiles of samples with f_{PSarc} of 0.31 and 0.25 fit the vesicle model (Fig. 2j-k), suggesting the majority presence of vesicles as the larger diameter population observed by DLS and TEM. SAXS was particularly important for the vesicles of 0.31 weight fraction (Fig. 2e), since the appearance of these structures deviated from the appearance more commonly observed for negatively stained vesicles

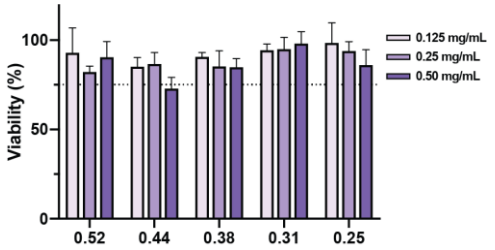

Fig 3 Cytotoxicity of the representative copolymer formulations in RAW 264.7 macrophages dosed from 0.125 mg/mL to 0.500 mg/mL. The dashed line highlights the 75% viability threshold.

reported in this study. SAXS modeling clarified this morphological ambiguity, with a good fit between the obtained scattering profile and a spherical vesicle model ($X^2 < 1$; Fig. 2j).

Together, these orthogonal analyses converge on a cohesive morphological description of the PSarc-*b*-PPS copolymer samples. Prototype polymer formulations with a f_{PSarc} above 0.38 resulted in a single monodisperse population of micelles, while formulations with a f_{PSarc} below 0.38 result in a second majority population of polymersomes (Fig. 2a). The polymers of f_{PSarc} = 0.38 appeared to exist at the border of the two morphologies, as the DLS and TEM profiles matched those of the polymersome samples, but the SAXS scattering profile best fit the core-shell model of the micelle samples. Overall, this work highlights the innate differences across the analytical methods as DLS and SAXS average across the population, while the visualization of TEM is able to focus on the distinct morphological characteristics of even minor subpopulations. These nanostructures were also able to encapsulate hydrophobic dyes ethyl eosin and DiI, which confirms the presence of a defined hydrophobic space to stably retain the cargo (Table S7). As confirmed from these techniques, this novel diblock PSarc-*b*-PPS copolymer is capable of forming diverse morphologies in aqueous media with definitive organic and aqueous lumens, which may accommodate the encapsulation of hydrophobic and hydrophilic therapeutics as observed for PEG-*b*-PPS.

To assess the toxicity of the assembled nanostructures to mammalian cells, we performed an MTT assay using RAW 264.7 macrophages after treatment with copolymer concentrations (0.125 - 0.50 mg/mL). These structures were largely non-toxic, as observed by the cell viability near or above 75% in each case (Fig. 3). Future use of these materials will require cell-specific toxicity studies relevant to the application of interest. However, the absence of toxicity in murine-derived macrophages, capable of extensive nanoparticle endocytosis,[27-29] gives reason to be optimistic on cellular interactions and new directions for biomedical applications.

In summary, we developed and optimized a screening workflow that utilizes a combinatorial library of polymer variants to minimize the material required to comprehensively assess the self-assembling properties of the new NCA-*b*-PPS polymer system. As a pilot example, we have shown that PSarc-*b*-PPS is a novel self-assembling copolymer capable of stably forming both micellar and vesicular morphologies in aqueous media. Our extensive characterization efforts suggest PSarc-*b*-PPS to potentially be a versatile diblock copolymer platform for nanocarrier fabrication, as it is amenable to the assembly of diverse morphologies via a scalable FNP methodology. Our pipeline is particularly well-suited for evaluating NCA-*b*-PPS materials but can be easily modified to investigate the supramolecular assembly space of other polymer systems. Overall, this work significantly advances our ability to develop novel self-assembling NCA-*b*-PPS block copolymers, which will help increase the diversity of nanocarrier platforms available for meeting unique drug delivery challenges.

Conflicts of interest

There are no conflicts to declare.

References

1 K. E. B. Doncom, L. D. Blackman, D. B. Wright, M. I. Gibson and R. K. O'Reilly, *Chem. Soc. Rev.*, 2017, **46**, 4119–4134.
2 Y. Shamay, J. Shah, M. Işık, A. Mizrachi, J. Leibold, *Nat Mater*, 2018, **17**, 361–368.
3 M. Frey, S. Bobbala, N. Karabin and E. Scott, *Nanomedicine*, 2018, **13**, 142.
4 G. Y. Tonga, K. Saha and V. M. Rotello, *Adv Mater*, 2014, **26**, 359–370.
5 J. Zagorski, J. Debelak, M. Gellar, J. A. Watts and J. A. Kline, *J Immunol*, 2003, **171**, 5529–5536.
6 A. Napoli, M. Valentini, N. Tirelli, M. Müller and J. A. Hubbell, *Nat Mater*, 2004, **3**, 183–189.
7 S. Yi, S. D. Allen, Y.-G. Liu, B. Z. Ouyang, X. Li, *ACS Nano*, 2016, **10**, 11290–11303.
8 A. E. Vasdekis, E. A. Scott, C. P. O'Neil, D. Psaltis and J. A. Hubbell, *ACS Nano*, 2012, **6**, 7850–7857.
9 E. Nicol, T. Nicolai and D. Durand, *Macromolecules*, 1999, **32**, 7530–7536.
10 S. Allen, O. Osorio, Y.-G. Liu and E. Scott, *J Control Release*, 2017, **262**, 91–103.
11 S. D. Allen, Y.-G. Liu, S. Bobbala, L. Cai, P. I. Hecker, *Nano Res.*, 2018, **11**, 5689–5703.
12 G. J. M. Habraken, K. H. R. M. Wilsens, C. E. Koning and A. Heise, *Polym. Chem.*, 2011, **2**, 1322–1330.
13 H. Lu, J. Wang, Z. Song, L. Yin, Y. Zhang, *Chem. Commun.*, 2014, **50**, 139–155.
14 A. R. Statz, A. E. Barron and P. B. Messersmith, *Soft Matter*, 2008, **4**, 131–139.
15 S. Bleher, J. Buck, C. Muhl, S. Sieber, S. Barnert, *Small*, 2019, **15**, e1904716.
16 X. Tao, H. Chen, S. Trepout, J. Cen, J. Ling, *Chem. Commun.*, 2019, **55**, 13530–13533.
17 H. Tanisaka, S. Kizaka-Kondoh, A. Makino, S. Tanaka, M. Hiraoka, *Bioconjugate Chem.*, 2008, **19**, 109–117.
18 A. Makino, R. Yamahara, E. Ozeki and S. Kimura, *Chem. Lett.*, 2007, **36**, 1220–1221.
19 D. Huesmann, O. Schäfer, L. Braun, K. Klinker, T. Reuter, *Tetrahedron Lett*, 2016, **57**, 1138–1142.
20 J. Liu and J. Ling, *J. Phys. Chem. A*, 2015, **119**, 7070–7074.
21 S. Cerritelli, C. P. O'Neil, D. Velluto, A. Fontana, M. Adrian, *Langmuir*, 2009, **25**, 11328–11335.
22 S. Bobbala, S. D. Allen, S. Yi, M. Vincent, M. Frey, *Nanoscale*, 2020, **12**, 5332–5340.
23 S. D. Allen, Y.-G. Liu, T. Kim, S. Bobbala, S. Yi, *Biomater. Sci.*, 2019, **7**, 657–668.
24 N. B. Karabin, S. Allen, H.-K. Kwon, S. Bobbala, E. Firlar, *Nat Commun*, 2018, **9**, 37.
25 F. Du, Y.-G. Liu and E. A. Scott, *Cel. Mol. Bioeng.*, 2017, **10**, 357–370.
26 S. D. Allen, S. Bobbala, N. B. Karabin and E. A. Scott, *Nanoscale Horiz.*, 2019, **4**, 258–272.
27 D. J. Dowling, E. A. Scott, A. Scheid, I. Bergelson, S. Joshi, *J Allergy and Clin Immunol*, 2017, **140**, 1339–1350.
28 S. Yi, X. Zhang, M. H. Sangji, Y. Liu, S. D. Allen, *Adv Funct Mater*, 2019, **29**, 1904399.
29 S. D. Allen, S. Bobbala, N. B. Karabin, M. Modak and E. A. Scott, *ACS Appl Mater Interfaces*, 2018, **10**, 33857–33866.

A robust pipeline of synthesis, self-assembly, and characterization was employed to optimize the fabrication of poly(sarcosine)-*b*-poly(propylene sulfide) nanostructures.

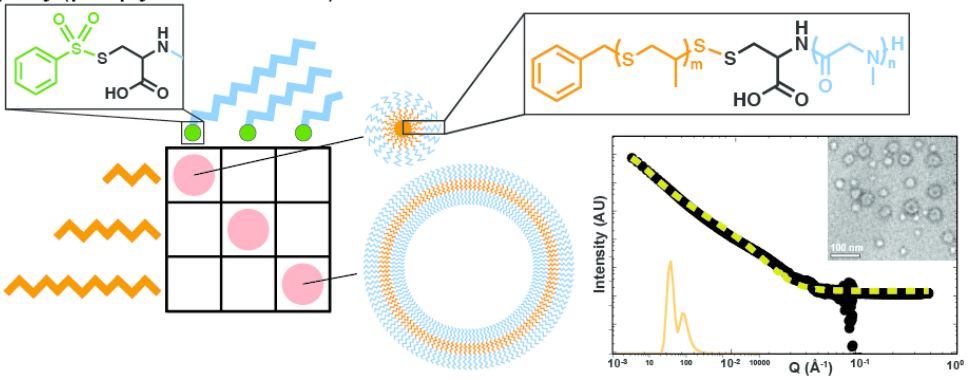

80x40mm (300 x 300 DPI)